Self-Diffusion in a Liquid Complex Plasma

S. Nunomura,* D. Samsonov, S. Zhdanov, and G. Morfill

Max-Planck-Institut für Extraterrestrische Physik, D-85740 Garching, Germany

(Received 26 June 2005; published 4 January 2006)

Self-diffusion has been experimentally studied in a two-dimensional underdamped liquid complex (dusty) plasma. It was found that the self-diffusion coefficient D increases linearly with the temperature T: $D/\omega_E a^2 = (0.019 \pm 0.007)(T/T_m - 1)$, where T_m, ω_E, and a are the melting temperature, the Einstein frequency, and the mean particle separation, respectively. No superdiffusion was observed, whereas a subdiffusion occurred at temperatures close to melting.

DOI: 10.1103/PhysRevLett.96.015003 PACS numbers: 52.27.Lw, 52.35.Fp

Complex plasmas are mixtures of macroscopic (usually spherical monodispersed micron-sized) grains with an ion-electron plasma. These grains charge up negatively and interact electrostatically with one another; they can be levitated and confined in a gas discharge and were shown to form ordered structures [1–4]. Complex plasmas can exist in different phase states, exhibit phase transitions [5,6], sustain waves [7–10], and conduct heat [11]. The motion of every grain can be easily observed with a video camera in real time and therefore a complex plasma can be used as a model system [5] of real solids, liquids, and gases at the kinetic level.

''Diffusion'' is the mixing of two different substances due to, e.g., the thermal motion of molecules, whereas ''self-diffusion'' refers to the motion of a single molecule in a pure substance. Experimental studies of self-diffusion in real fluids are very difficult and use indirect methods such as nuclear magnetic resonance [12], which do not resolve the motion of individual molecules. In molecular-dynamics simulations, self-diffusion coefficient can be easily determined, and it was the subject of many simulation studies including Lennard-Jones model fluids [13] and Yukawa systems [14–17]. From these simulations, a simple scaling law for the self-diffusion coefficient has been found [17]:

$$D/\omega_E a^2 = 0.0132(T/T_m - 1) + 0.00317,$$

where ω_E is the Einstein frequency, a is the particle separation, and T_m is the melting temperature. This scaling is obtained in the range of $T/T_m - 1 \lesssim 10$. The Einstein frequency is the characteristic frequency of oscillations of particles in the solid phase, defined by

$$\omega_E^2 = \frac{1}{3m}\sum_{i \neq j} \triangle \phi_{ij},$$

where m is the mass of the particles and ϕ_{ij} is the particle interaction potential. The value of $D/\omega_E a^2$ is almost independent of the screening parameter $\kappa = a/\lambda_D$, where λ_D is the screening length. The self-diffusion coefficient can be determined using the Einstein relation [18] if the trajectories of the moving particles are resolved:

$$D = \frac{1}{2nN}\sum_i \lim_{t\to\infty} \langle \Delta x_i^2(t) \rangle / t,$$

where Δx_i^2 is the mean-square displacement (MSD) of ith particle, n is the dimension of the space ($n = 2$ in our case), and N is the number of particles.

Diffusive motion of particles has been reported in early complex plasma experiments [5,6]. Later experiments in multilayer quasi-two-dimensional complex plasmas [19–22] studied self-diffusion using MSD curves of particles. It was found that at the short time scales [22] the particle motion was ballistic (MSD $\propto t^2$), at longer times it was subdiffusive due to caged motion, whereas at even longer times it became quasidiffusive, i.e., MSD $= Dt^b$, where coefficient $b = 1$ would correspond to normal diffusion. A range of subdiffusive ($b < 1$) to superdiffusive ($b > 1$) motion was observed at intermediate time scales which tended to become normal or weakly super- ($b = 1$–1.3) diffusive at longer times [19–22].

In this Letter, we present experiments on self-diffusion of particles in a monolayer (two-dimensional) liquid complex plasma, and report measurements of the self-diffusion coefficient. Unlike the previous experiments, ours were performed at a very low gas pressure (1 Pa, or 7.5 mTorr), which ensured that the phonon decay length was $\simeq 20a$ for longitudinal phonons (a is the interparticle distance) and $\simeq 5a$ for transverse phonons. The phonon decay lengths in previous experiments (performed at 250–500 mTorr), were at least 30 times shorter than in ours and smaller than the interparticle distance. Long phonon decay lengths ensure that the complex plasma behaves like real solids and liquids (and not like colloids), where transport phenomena rely on phonons. We also performed molecular-dynamics simulations which agreed well with our experiments.

The experiments were performed in a capacitively coupled 13.56 MHz radio-frequency (rf) discharge. We used the experimental setup (shown in Fig. 1), which is described in detail in Ref. [10]. A plasma was generated by applying a rf power of 2 W to the lower disk electrode. An argon flow rate of 1.5 sccm maintained the gas pressure in the chamber at $p = 1.0$ Pa.

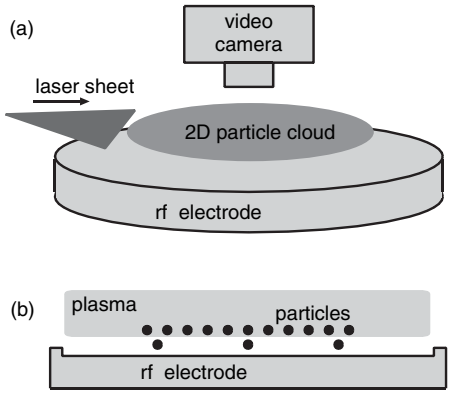

FIG. 1. Sketch of apparatus. (a) Oblique view. Spherical particles charge negatively and form a monolayer levitating in the plasma sheath above the lower electrode. They are illuminated with a horizontal sheet of a doubled Nd:YAG laser (532 nm) and viewed from the top with a video camera. (b) Side view. The heating of the particle suspension was provided by an instability caused by a ''perturbation layer'' of heavier particles levitated below the main layer. Increasing the number of particles in the perturbation layer produced a higher kinetic temperature in the main layer.

To make a monolayer particle suspension, we injected monodisperse plastic microspheres into the plasma. The particles levitated in the plasma sheath above the rf electrode, where they formed a hexagonal lattice. The lattice was composed of ≈ 5000 particles and its diameter was ≈ 7 cm (particle separation $a = 1.01$–1.07 mm). The particles had a diameter of 8.9 ± 0.1 μm, and a mass of $m = 5.57 \times 10^{-13}$ kg. The particle charge and the shielding parameter were determined as $Q = 17000e \pm 15\%$ and $\kappa \equiv a/\lambda_D = 1.0$ from the spectral analysis of phonons in the lattice [see Refs. [7,8]]. The Einstein frequency was calculated assuming an ideal hexagonal lattice, Yukawa interaction, and taking into account the interaction of the particles separated by up to 20 average interparticle distances. It was found that $\omega_E = 13.4\ \mathrm{s}^{-1}$ for our lattice.

The kinetic temperature and the phase state of the particle suspension were controlled by adding a small number of larger particles (with diameter 12.7 ± 0.15 μm and a mass of 1.62×10^{-12} kg). The heavier grains were levitated in the plasma sheath in a ''perturbation layer'' several hundred μm below the main layer [Fig. 1(b)] and were spontaneously accelerated like in a Mach cone experiment [23]. Unlike in that experiment, they often collided with one another and heated the lattice instead of producing wakes. The kinetic temperature of the main particle layer increased with the number of perturbing particles. In our experiments these comprised up to 10% of the number of grains in the main layer. Neither Q nor λ_D were affected by this perturbation layer, because it is located downstream of the supersonic ion flow in the plasma sheath. The inhomogeneity of the temperature across the field of view was typically less than 20%. Occasional hot spots at the edges were cropped. They covered only a small fraction of the field of view.

To observe the thermal motion of the particles, we illuminated the suspension with a horizontal (0.2–0.3 mm thin) sheet of laser light, and viewed it by a digital video camera from the top window. 512 images were recorded in each sequence at 22–154 frames per second. The particle positions were then identified and traced from one frame to the next. The particle velocities were calculated from their displacements in two consecutive frames. The kinetic temperature of the particles was calculated from the width of the velocity distribution function, which was Maxwellian.

As the kinetic temperature of the particles increased, the suspension melted at around $T_m = 14.5$ eV (corresponding to a coupling parameter $\Gamma_{\mathrm{eff}} = 10.6$). The coupling parameter Γ [1] is the ratio of the potential energy of the particle interaction to the particle kinetic energy. Γ is often normalized by the exponential of the screening parameter κ: $\Gamma_{\mathrm{eff}} = \Gamma \exp(-\kappa)$ [16]. The coupling parameter determines the phase state of the system. Large Γ_{eff} correspond to solids, small values to gases, and $\Gamma_{\mathrm{eff}} \simeq 1$ characterizes liquids. The solid-liquid phase transition was reported to occur at coupling parameters ranging from $\Gamma = 137$ for a classical 2D layer of electrons on a surface of liquid helium [24] to $\Gamma = 10$ in a 3D molecular-dynamics simulation of a hexagonal crystal in a flowing plasma, where the attractive force of the wakefield was responsible for low Γ [25].

After the melting transition at $T_m = 14.5$ eV, the motion of the particles changed from oscillations around equilibrium positions to diffusion, and the structure became more disordered [see Figs. 2(a)–(c) of Ref. [10]]. The pair correlation functions [see Figs. 2(d)–(f) of Ref. [10]] indicate that the suspension is highly ordered (solid phase) at 0.037 eV, partly melted at 14.5 eV, and in a liquid state at 54.9 eV.

To study the thermal motion of particles, their mean-square displacements (MSD) were computed from their trajectories using the entire field of view (with hot spots at the edges cropped). Figure 2 shows MSD as a function of time t at various kinetic temperatures. Here, MSD in the solid phase at $T = 5.4$ eV is shown for comparison. On short time scales ($\omega_E t \lesssim 1$) the particles move ballistically and MSD depends quadratically on time. On long time scales, the motion is diffusive (except for the solid phase, where it is limited by the size of the lattice cell) and MSD grows linearly with time. A small dip in the MSD slope (subdiffusion) for the temperatures above melting (Fig. 2) at time $t = 0.1$–0.2 s might be due to caged motion.

The self-diffusion coefficient can be determined from the slope of the MSD curve (Fig. 2) at large time (where MSD $\propto t$). We fitted these curves with a function $c_1 \omega_E^{-1} (t\omega_E)^{c_2}$ and plotted the coefficients c_1 and c_2 in Fig. 3. The value of $c_2 = 1$ indicates that the MSD depends linearly on time and the particle motion is diffusive, thus c_1 can be used to determine the diffusion coefficient in this case. At a temperature $T < 25$ eV, $c_2 < 1$ and therefore the particle motion is ''subdiffusive''. It is interesting that the particle motion becomes diffusive at a temperature of and

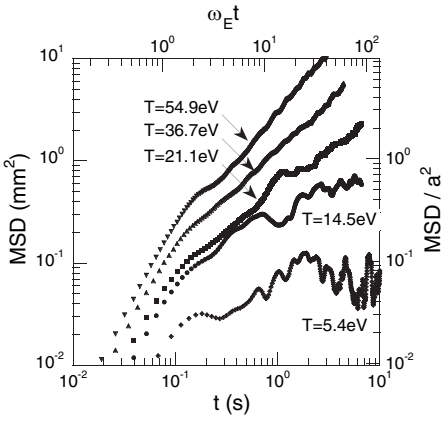

FIG. 2. Mean-square displacement (MSD) in the solid and liquid phases at different kinetic temperatures. On the short time scales ($\omega_E t \lesssim 1$), the MSD is proportional to t^2, which corresponds to ballistic motion of the particles. On the long time scales ($\omega_E t \gtrsim 1$), MSD increases linearly with time in the liquid phase ($T = 54.9$ eV, 36.7 eV, and 21.1 eV) indicating diffusion. MSD of the solid ($T = 5.4$ eV) is almost constant at $\omega_E t \gtrsim 1$, since it is limited by the crystal cell size.

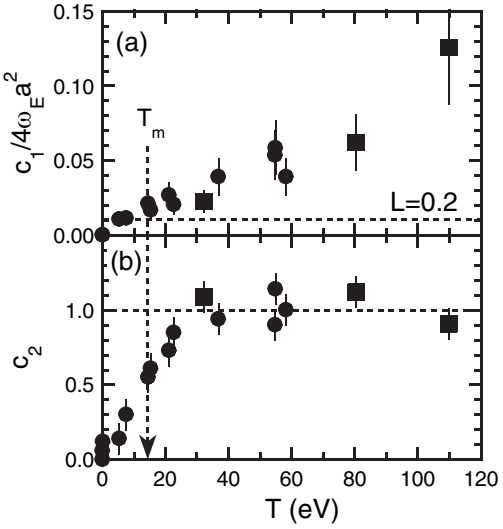

FIG. 3. Coefficients (a) c_1 and (b) c_2 obtained from the least-squares fits of the MSD (at $\omega_E t \gtrsim 1$) to a function $c_1 \omega_E^{-1} (t\omega_E)^{c_2}$ vs kinetic temperature T. c_1 is normalized by $4\omega_E a^2$, and it equals the normalized diffusion coefficient if $c_2 \simeq 1$ (at $T \gtrsim 25$ eV). The filled circles (●) are the data at a gas pressure of $p = 1.0$ Pa. The filled squares (■) are the data for a denser particle suspension ($a \simeq 0.75$ mm) at higher gas pressures of $p = 3.4$, 2.2, and 1.5 Pa. At low temperature, both c_1 and c_2 become equal to zero indicating that there is no diffusion in the solid phase. At 5 eV $< T <$ 25 eV the particle motion is sub-diffusive ($c_2 < 1$). The melting temperature T_m is marked by a vertical dashed line (a), (b), and the value of $c_1/(4\omega_E a^2)$ corresponding to the Lindemann parameter $L = 0.2$ by a horizontal dashed line (a).

above 25 eV, i.e., significantly higher than the melting temperature 14.5 eV. We attribute this to the coexistence of two different phases [26] liquid and solid (or hexatic) at the temperatures close to melting 14.5 eV $< T <$ 25 eV. This is consistent with the Kosterlitz-Thouless-Halperin-Nelson-Young (KTHNY) melting theory, which predicts two phase transitions: solid hexatic and hexatic liquid [see Ref. [27] and references therein].

Figure 4(a) shows the temperature dependence of the self-diffusion coefficient, determined from c_1 and normalized by $\omega_E a^2$. This figure includes the data obtained for different experimental conditions and molecular-dynamics simulations as indicated in the figure caption. The simulation method is described in Ref. [8].

The temperature dependence of the self-diffusion coefficient [Fig. 4(a)] can be used to determine the lattice melting temperature T_m. A two parameter fit to a function $D/\omega_E a^2 = \alpha(T/T_m - 1)$ yields the value $T_m = 14.3 \pm 7.8$ eV. The error bar is large due to two reasons: first, we have to extrapolate the data to lower temperatures; second, there are only two data points at high temperature and they have a large scatter. In order to reduce the error of the second fit coefficient α we also estimated the melting temperature independently, using a visual observation of the particle motion under conditions identical to our previous experiment [10] and determined that the melting temperature has a similar value of 14.5 eV. A one parameter fit with $T_m = 14.3$ yields $\alpha = 0.019 \pm 0.007$, which is more precise than the one obtained from a two parameter fit.

The lattice melting temperature can be also estimated independently by using the semiempirical (and notably not very reliable [28,29]) Lindemann criterion, which predicts melting when the mean-square displacement $\langle \Delta x^2 \rangle$ exceeds some fraction of the interparticle distance a: $\langle \Delta x^2 \rangle / a^2 > L^2$, where L is the Lindemann parameter. The value of L ranges from 6% to 21% for different solids [30,31] to $\approx 30\%$ (in a modified form) for Coulomb and Lennard-Jones systems [32]. For Yukawa solids $L =$ 16%–19% is most often used [33–35]. We assume that each particle in a 2D hexagonal lattice oscillates in a parabolic potential produced by its surrounding particles (up to $20a$ away); i.e., we use the harmonic approximation [14,36]. Since the particles' kinetic temperature is equal to their average potential energy at the mean-square displacement corresponding to the Lindemann parameter, and the potential energy can be expressed in terms of ω_E, we obtain the melting temperature:

$$T_m = (3/4)\omega_E^2 m a^2 L^2.$$

Using $L = 16\%$–19% we obtain $T_m = 12$–17 eV, which agrees with our observations and fit value.

The measurements of our 2D normalized self-diffusion coefficient, given approximately by the fit

$$D/\omega_E a^2 = (0.019 \pm 0.007)(T/T_m - 1),$$

agree quite well with the 3D molecular-dynamics simulations of Refs. [14,15,17], where D was predicted to increase linearly with temperature at large T/T_m. Figure 4(b) presents the self-diffusion coefficient versus $T/T_m - 1$.

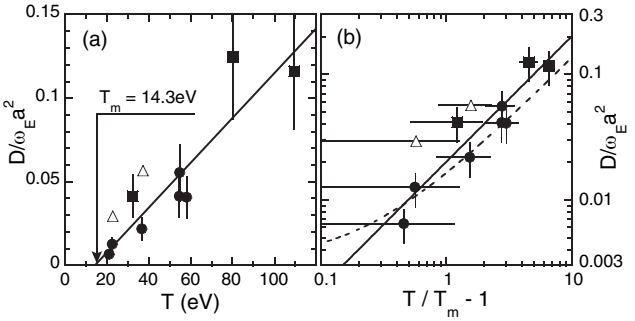

FIG. 4. Normalized self-diffusion coefficient $D/\omega_E a^2$ in a liquid complex plasma. (a) $D/\omega_E a^2$ vs temperature T. (b) The same data plotted vs $T/T_m - 1$ to facilitate the comparison with the simulations of Refs. [14,15,17]. The filled circles (●) are the data at a gas pressure of $p = 1.0$ Pa. The filled squares (■) are the data for a denser particle suspension ($a \simeq 0.75$ mm) at higher gas pressures of $p = 3.4$, 2.2, and 1.5 Pa. For comparison, the self-diffusion coefficients from our 2D MD simulations are shown as open triangles (△). The solid line represents a least square fit with a function $D/\omega_E a^2 = (0.019 \pm 0.007)(T/T_m - 1)$, where the melting temperature $T_m = 14.3$ eV. The measurements agree with the results obtained in 3D MD simulations of Yukawa systems [14,15,17], which are given by the dashed line.

The horizontal error bars are due to the uncertainty in the melting temperature. The coefficient α in our 2D experiments and simulations is larger than that in 3D systems [14,15,17] by about 66%. However, within the measurement errors [see Fig. 4(b)] the results are compatible.

Our results disagree with those of Refs. [19–22]. We found no superdiffusion, and the motion was subdiffusive near the melting temperature. This agrees well with the simulations of Ref. [14], where no superdiffusion was found and the subdiffusion near melting is explained by caged motion. The disagreement with Refs. [19–22] is most likely due to neutral damping, which was 40–100 times higher in their case. The simulations of Ref. [14] were performed for the underdamped Yukawa systems [undergoing ballistic dynamics in the terminology of Ref. [14]] and they are not expected to describe the dynamic behavior (such as diffusion) of over-damped systems with Brownian dynamics. The damping rate in the experiments of Refs. [19–22] ($\nu_d \approx$ 60–100 s^{-1}) is higher than the oscillation frequency [$\omega_{osc} = \sqrt{3}\omega_E \approx 60$ s^{-1}, estimated using parameters of Ref. [20], or $\omega_{osc} \approx 30$ s^{-1} in Ref. [22]] and thus these systems are critically damped or over-damped. Our system has $\nu_d = 1.37$ $s^{-1} \ll \sqrt{3}\omega_E = 23.4$ s^{-1} and therefore it is clearly underdamped. Another reason for disagreement is that our experiment is performed with a monolayer, while the experiments of Refs. [19–22] were done with vertical chains of 2–3 [22] to more than 25 particles [19]. Systems of vertical chains are subject to Schweigert instability [37].

The self-diffusion in 2D underdamped liquid complex plasmas was studied by measuring the mean-square displacement of particles at various kinetic temperatures. It was demonstrated that motion was subdiffusive near the melting point, and it becomes diffusive at higher temperatures. The self-diffusion coefficient was found to increase linearly with the temperature. These results agree with our MD simulations as well as with the simulations of Refs.[14,15,17].

S. N. acknowledges the Japan Society of the Promotion of Science.

*Present address: Research Center for Photovoltaics, National Institute of Advanced Industrial Science and Technology, Tsukuba, Ibaraki 305-8568, Japan.

[1] H. Ikezi, Phys. Fluids **29**, 1764 (1986).
[2] J. H. Chu and L. I, Phys. Rev. Lett. **72**, 4009 (1994).
[3] Y. Hayashi and K. Tachibana, Jpn. J. Appl. Phys. **33**, L804 (1994).
[4] H. Thomas *et al.*, Phys. Rev. Lett. **73**, 652 (1994).
[5] H. Thomas and G. Morfill, Nature (London) **379**, 806 (1996).
[6] A. Melzer *et al.*, Phys. Rev. E **53**, 2757 (1996).
[7] S. Nunomura *et al.*, Phys. Rev. Lett. **89**, 035001 (2002).
[8] S. Zhdanov *et al.*, Phys. Rev. E **68**, 035401(R) (2003).
[9] A. Melzer, Phys. Rev. E **67**, 016411 (2003).
[10] S. Nunomura *et al.*, Phys. Rev. Lett. **94**, 045001 (2005).
[11] S. Nunomura *et al.*, Phys. Rev. Lett. **95**, 025003 (2005).
[12] H. Carr and E. Purcell, Phys. Rev. **94**, 630 (1954).
[13] K. Meier *et al.*, J. Chem. Phys. **121**, 9526 (2004).
[14] M. Robbins *et al.*, J. Chem. Phys. **88**, 3286 (1988).
[15] Y. Rosenfeld *et al.*, Phys. Rev. Lett. **75**, 2490 (1995).
[16] S. Hamaguchi *et al.*, Phys. Rev. E **56**, 4671 (1997).
[17] H. Ohta and S. Hamaguchi, Phys. Plasmas **7**, 4506 (2000).
[18] H. Gould and J. Tobochnik, *An Introduction to Computer Simulation Methods* (Addison-Wesley, Reading, MA, 1988), Vol. I.
[19] W.-T. Juan and L. I, Phys. Rev. Lett. **80**, 3073 (1998).
[20] W.-T. Juan *et al.*, Phys. Rev. E **64**, 016402 (2001).
[21] Y.-J. Lai and L. I, Phys. Rev. Lett. **89**, 155002 (2002).
[22] R. A. Quinn and J. Goree, Phys. Rev. Lett. **88**, 195001 (2002).
[23] D. Samsonov *et al.*, Phys. Rev. Lett. **83**, 3649 (1999).
[24] C. C. Grimes and G. Adams, Phys. Rev. Lett. **42**, 795 (1979).
[25] F. Melandsø, Phys. Rev. E **55**, 7495 (1997).
[26] X. Zheng and J. Earnshaw, Europhys. Lett. **41**, 635 (1998).
[27] R. A. Quinn and J. Goree, Phys. Rev. E **64**, 051404 (2001).
[28] A. Hunt, J. Phys. Condens. Matter **4**, L429 (1992).
[29] G. Wolf and R. Jeanloz, J. Geophys. Res. **89**, 7821 (1984).
[30] E. Zarochentsev *et al.*, Sov. Phys. Solid State **18**, 239 (1976).
[31] J. Dobnikar *et al.*, J. Chem. Phys. **119**, 4971 (2003).
[32] V. Bedanov *et al.*, Sov. Phys. Solid State **27**, 1325 (1985).
[33] M. Stevens and M. Robbins, J. Chem. Phys. **98**, 2319 (1993).
[34] E. Meijer and D. Frenkel, J. Chem. Phys. **94**, 2269 (1991).
[35] H. Lowen *et al.*, Phys. Rev. Lett. **70**, 1557 (1993).
[36] D. Hone *et al.*, J. Chem. Phys. **79**, 1474 (1983).
[37] V. Schweigert *et al.*, Phys. Rev. E **54**, 4155 (1996).